THE JOURNAL OF PHYSICAL CHEMISTRY C

Article

pubs.acs.org/JPCC

First-Principles Prediction of Oxygen Reduction Activity on Pd−Cu−Si Metallic Glasses

Zhengzheng Chen,[†] Yiyi Yang,[‡] Sharvan Kumar,[‡] and Gang Lu*[,†]

[†]Department of Physics and Astronomy, California State University Northridge, Northridge, California 91330, United States

[‡]School of Engineering, Brown University, Providence, Rhode Island 02912, United States

Supporting Information

ABSTRACT: We carry out first-principles simulations to assess the potential of Pd−Cu−Si metallic glasses as catalysts for oxygen reduction reaction (ORR) using oxygen adsorption energy (E_O) as a descriptor. We find that the substitution of Cu on crystalline Pd(111) surface improves the ORR activity while the substitution of Si on the surface is in general detrimental to the ORR activity. Compressive strains are found to weaken oxygen binding on the surface and thus enhance the ORR activity. On the basis of the analysis of E_O distribution on the Pd metallic glasses surfaces, we find that for Si-deficient adsorption sites, the local ORR activity could exceed that on pure Pd surface, while Si-rich sites exhibit a rather poor ORR activity. The Pd metallic glasses can sustain a much higher compression than the crystalline counterpart, thus their ORR activity can be improved substantially under a large compression. It is predicted that low-Si Pd metallic glasses could be excellent ORR catalysts under compression.

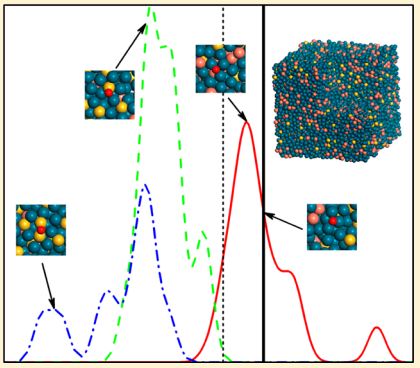

INTRODUCTION

Oxygen reduction reaction (ORR) is a key chemical reaction underlying diverse applications in energy conversion, metal corrosion and biology. Significant recent interest has been devoted to ORR in electrochemical devices such as proton exchange membrane fuel cells (PEMFC) and metal-air batteries.[1−4] Essential to these devices is the development of superior ORR catalysts that have high catalytic activity, large surface area and excellent durability. The conventional Pt/C catalysts in PEMFC, despite their high catalytic activities, suffer from substantial loss of electrochemical surface area (ECSA) owing to the formation of carbides and coarsening of Pt nanoparticles during the operation of the fuel cells.[5,6] Although nanostructured materials could potentially overcome this problem,[7−10] their fabrication processes are often too complicated to allow for highly scalable applications. Recently, Pt-based metallic glasses (Pt-MGs) have emerged as promising catalysts for ORR[11] thanks to their high strength, excellent castability and superior resistance to corrosion and wear.[12−16] In particular, Pt-MG nanowires can be fabricated in an economical and scalable manner leveraging the excellent castability of the metallic glasses;[11] the Pt-MG nanowires have large surface area and exhibit outstanding durability—the total ECSA loss is only 4% after 1000 cycles, much lower than 60% loss in the conventional Pt/C catalysts.

Inspired by this progress, we carry out first-principles simulations to explore the potentials of other metallic glasses as ORR catalysts. In this paper, we focus on Pd−Cu−Si metallic glasses (Pd-MGs in short) because they were among the first metallic glasses fabricated in millimeter scales with low cooling rates.[17−20] Moreover, by replacing more expensive Pt with Pd, the Pd-MGs could significantly reduce the cost of the fuel cells if their catalytic activity remains high. Nanostructured Pd-MGs could possess exceptional mechanical stability and large surface area—both are desirable properties for ORR catalysts. Finally, recent experiments have shown that the addition of Cu to pure Pd could lead to much enhanced ORR activity,[21,22] laying the groundwork for our investigation. Here, we show that Pd−Cu−Si metallic glasses can offer superior ORR activities than pure Pd. More importantly, the catalytic activities can be tuned by applying surface strains to them, offering an avenue to further improve their ORR activities. It has been known for a long time that active straining can change molecular adsorption energies on a metal surface and modify its catalytic activity.[23] However, this principle has not been exploited in practice owing to low yield strains of metal surfaces (~0.2%). For example, in order to change the ORR activity on Pd or Pt substantially, it is necessary to shift the oxygen adsorption energy by a few tenth of an electronvolt (0.2−0.4 eV). This corresponds to a surface strain on the order of a few percent (2−4%), which is 1 order of magnitude greater than the typical yield strain of metals. Such a large strain would cause the metal surface to deform plastically, generating dislocations and other lattice defects that would relax the elastic strain. As a result, the metal surface loses its ability to tune the catalytic activity. In contrast to crystalline metals, metallic glasses have no dislocations or grain boundaries and the normal plastic deformation channels are absent thanks to

Received: August 26, 2014
Revised: November 10, 2014
Published: November 20, 2014

   dx.doi.org/10.1021/jp508636y | J. Phys. Chem. C 2014, 118, 28609−28615

their amorphous nature.[24] Hence, metallic glasses possess high elastic limits and can sustain much larger strains than their crystalline counterparts.[25−27] It is therefore of great scientific and technological interest to examine whether and how surface strains can substantially enhance the ORR activity of metallic glasses.

It has been well established that oxygen adsorption energy E_O is a good descriptor for ORR activity. For example, it has been shown that the well-known "volcano" relationship can be obtained by plotting experimentally measured ORR activities as a function of E_O, which lends strong support to E_O as an ORR descriptor.[28−31] Note that these measured ORR activities are from different experimental groups on a variety of catalysts. To establish E_O as an ORR descriptor theoretically, one has to resort to first-principles density functional theory (DFT) calculation in conjunction with microkinetic models as pioneered by Nørskov et al.[28] Central to electrochemical reactions such as ORR is the free energy diagram as a function of electrode potential including all intermediates. Nørskov et al. have determined such free energy diagrams for ORR in the presence of water and pH values using DFT calculations although they did not find these effects to be important for obtaining qualitative trends.[28] On the basis of the free energy diagrams, it is concluded that for metals that bind oxygen too strongly, the reaction rate is limited by the removal of adsorbed O and OH species. For metal surfaces that bind oxygen too weakly, the reaction rate is limited by the dissociation of O_2, i.e., the transfer of electrons and protons to adsorbed O_2. More importantly, it was recognized that both rate-limiting mechanisms can be characterized by E_O.[30] In particular, it was shown that the overpotential of ORR could be linked directly to the proton and electron transfer to adsorbed oxygen or hydroxide at the electrode potential where the overall cathode reaction is at equilibrium, thus directly linked to E_O.[28] The general validity of E_O as an ORR descriptor has been demonstrated for dozens of transition metals and their alloys.[28,30,32] The universal relationship between E_O and ORR activity stems from the similarity among the transition state structures[33] and the scaling relations between E_O and E_{OHx}(the adsorption energy of OH species);[34] the latter justifies the use of E_O as a descriptor in multiple-electron reduction of oxygen. However, owing to limitations of DFT and approximations in the kinetic models, E_O is only expected to provide *semi-quantitative* predictions, such as general trends in ORR activities. Indeed, E_O has been used successfully to screen and design ORR catalysts with experimental confirmations.[32,35] For instance, Nørskov et al. calculated E_O on the closest-packed surfaces of 13 metals using DFT calculations with the plane-wave pseudopotential method. They have successfully reproduced the "volcano" plot with Pt and Pd being the best ORR catalysts. Using the similar first-principles simulations and QM/MM multiscale modeling, Zhang et al. have examined the effect of strain on ORR activity in core/shell nanoparticles based on the analysis of E_O as a function of strain.[35]

In this paper, we assess ORR activities of the Pd-MGs using E_O as a descriptor. First, we perform DFT calculations to evaluate E_O on crystalline Pd−Cu and Pd−Si (111) surfaces, providing a basic understanding of the ORR activity on chemical compositions. The results on Pd−Si alloys are consistent with experimental observations. We then apply strains to these surfaces and examine how strain influences the ORR activity. Subsequently we move to the Pd-MGs and explore the composition- and strain-dependence of ORR activity on a large number of metallic glass surfaces. On the basis of analysis of E_O distribution as a function of strain and chemical composition, we predict that low-Si content Pd-MGs could be excellent ORR catalysts under large compressive strains.

MODELS AND METHODOLOGY

The atomic structures of Pd-MGs are generated by molecular dynamics (MD) simulations with LAMMPS package[36] and EAM potentials.[37,38] Two alloy compositions, $Pd_{77}Cu_{17}Si_6$ (Si_6) and $Pd_{77}Cu_6Si_{17}$ (Si_{17}), are chosen as examples to represent a relatively low and high Si-content Pd-based metallic glasses (Pd-MGs). The dimensions of the MD supercell are 62 × 62 × 62 Å^3 with 13310 atoms randomly arranged therein. The amorphous alloys are first heated up to 4000 K and then annealed to 300 K with a cooling rate of 10^{13} K s^{-1} and finally equilibrated at 300 K for 200 ps by employing with the Nośe−Hoover thermostat.[39] The radial distribution function (RDF), $g(r)$ of both Si_6 and Si_{17} Pd-MG are displayed in Figure 1. Two $g(r)$ peaks are present for Si_{17} Pd-MG, corresponding to the first and second nearest neighbor (NN) distance of 2.44 and 2.72 Å, respectively. Experiments on $Pd_{75.1}Cu_{6.6}Si_{18.3}$ metallic

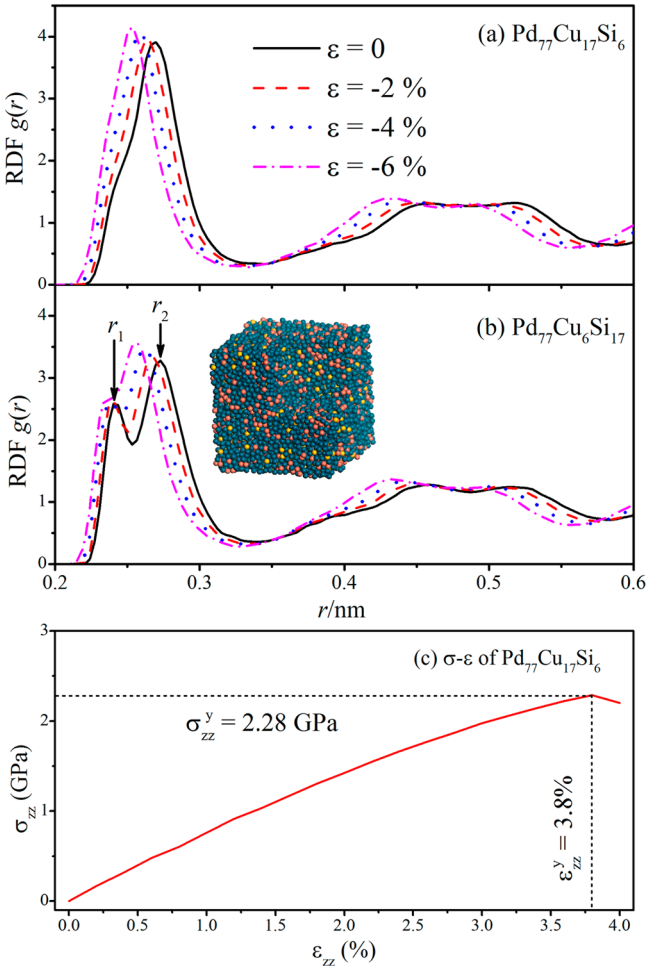

Figure 1. Radial distribution function $g(r)$ of (a) Si_6 Pd-MG and (b) Si_{17} Pd-MG in the absence and the presence of hydrostatic pressures. Inset shows a typical MD snapshot of the atomic structure. Blue, pink, and yellow spheres represent Pd, Cu, and Si atoms, respectively. (c) Stress−strain relationship for Si_6 Pd-MG under a uniaxial tension in the z direction.

dx.doi.org/10.1021/jp508636y | J. Phys. Chem. C 2014, 118, 28609−28615

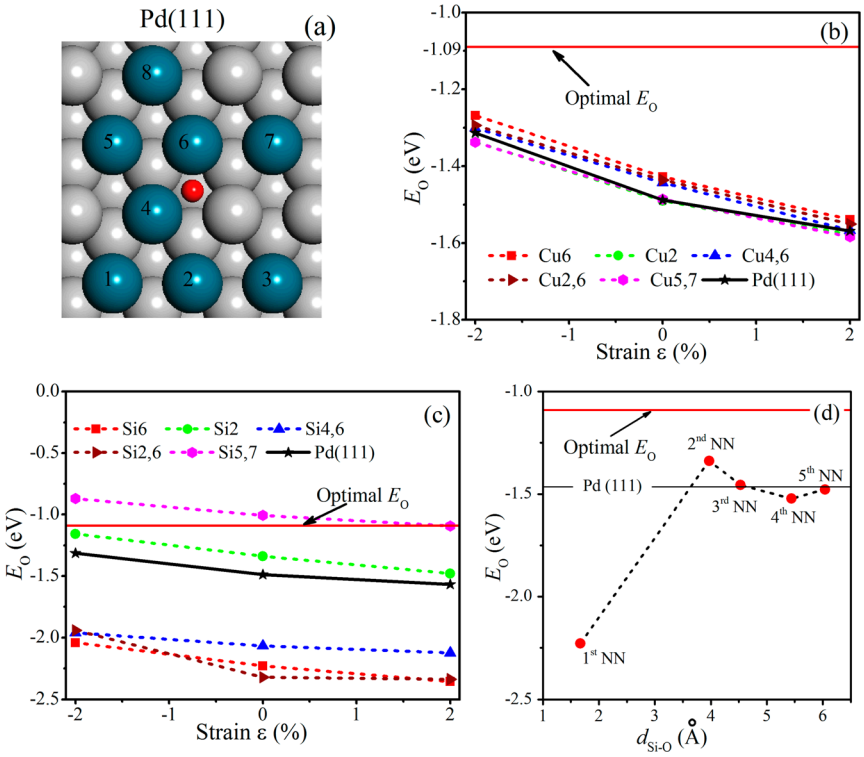

Figure 2. (a) Atomic structure of Pd(111) surface. An oxygen atom (small red sphere) is adsorbed on an fcc hollow site. Blue spheres with numerical labels indicate the substitutional sites considered in the calculations. (b) E_O as a function of surface strain with different Pd atoms substituted by Cu. The results for the pure Pd surface are shown in the solid black line. (c) E_O as a function of surface strain with different Pd atoms substituted by Si. (d) E_O as a function of d_{Si-O}; the horizontal black line represents the E_O value on the pure Pd(111) surface. The positive (negative) strain indicates tension (compression). The red solid line in parts b–d represents the optimal E_O value.

glass[40] have also found two $g(r)$ peaks with the first and second NN distance as 2.42 and 2.80 Å, respectively. The excellent agreement between the simulation and the experiments suggests that the MD simulations can provide a reasonable description for the atomic structure of the Pd-MGs.

In this paper, E_O is defined as follows:

$$E_O = E(\text{Surf} + \text{O}) - E(\text{Surf}) - \mu_O \quad (1)$$

Here E(Surf+O) and E(Surf) is the total energy of the surface slab with and without an adsorbing O atom, respectively, and $\mu_O = E_{O_2}/2 = -4.887$ eV. A more negative E_O value indicates a stronger chemisorption. E_O values are calculated based on the DFT using PBE exchange-correlation functional[41,42] and projected augmented wave approach[43] as implemented in the VASP package.[44,45] The energy cutoff is 400 eV, and only Γ point is considered in the calculations owing to the amorphous nature of the metallic glasses. We have also sampled the Brillouin zone using 2 × 2 × 1 Monkhorst–Pack k-point mesh[46] for 13 different oxygen adsorption sites, but find the changes in E_O less than 0.05 eV for each of them. Hence the Γ-point is adequate for obtaining converged results. The atomic geometries are optimized until the forces on all unconstrained atoms are less than 0.03 eV Å^{-1}.

RESULTS AND DISCUSSION

Crystalline Pd(111) Surface. We first determine the optimal E_O value to be −1.09 eV, which corresponds to the maximal ORR activity on metal surfaces as established in previous works.[28] We next examine oxygen adsorption on crystalline Pd(111) surface with substitutional Cu and Si atoms. As shown in Figure 2a, a 4-layer 3 × 3 slab model (72 atoms) is employed to represent the crystalline surface with the lattice constant a = 3.953 Å, which is 1.6% larger than the experimental value of 3.891 Å. The bottom two atomic layers are fixed at their equilibrium bulk structure during the atomic relaxation. An oxygen atom is placed at an fcc-hollow site which is the most stable adsorption site. Seven substitutional sites labeled from 1 to 7 are considered at which the Pd atoms are replaced by either Cu or Si. The oxygen adsorption energies E_O are calculated in the absence and presence of biaxial strains and the results are displayed in Figure 2b–d. The horizontal redline in the figures represents the optimal E_O for ORR, serving as a target (or standard) for designing (or ranking) ORR catalysts. In the absence of the surface strain, the substitutional Cu shifts E_O slightly toward the optimal value depending on the local adsorption structure. This result agrees with experimental observations[21,22] and can be attributed to the change of d-band center due to the charge transfer between Pd and Cu.[47]

The effect of Si substitution is more complicated and strongly dependent on the local adsorption structure. As shown in Figure 2c, in general Si is detrimental to ORR because it bonds too strongly to oxygen and E_O is 1.0 to 1.4 eV lower than the optimal value. The general detrimental effect of Si on ORR activities has also been observed experimentally on a series of Pd–Si thin films with varying Si contents. As shown in Figure S1 (Support Information), the cyclic voltammetry (CV) curves of the Pd–Si alloys exhibit a monotonic decrease of ORR activity as Si content is increased. There are, however, some exceptions where E_O is actually higher than the optimal value. To understand the exceptions, we plot E_O as a function of Si–O distance, d_{Si-O}, on Pd(111) surface. As shown in Figure 2d, a

dx.doi.org/10.1021/jp508636y | J. Phys. Chem. C 2014, 118, 28609–28615

damped oscillation of E_O is observed as a function of d_{Si-O}. Beyond the second NN, Si substitution has a negligible effect on E_O and thus can be ignored. Although the second NN Si atoms have a weaker bonding to oxygen, their effect on ORR is overcompensated by a much stronger chemisorption of oxygen to the first NN Si. However, if Si concentration is low, the first NN Si atoms could be exhausted or fully covered by oxygen. As a result, the remaining oxygen would have to bond with the second NN Si, which could lead to an enhanced ORR activity. To see this effect more clearly, we present the bonding charge density distribution $\rho(r)$ on the Pd(111) surface with an O atom placed at the first NN (Figure 3a) and second NN

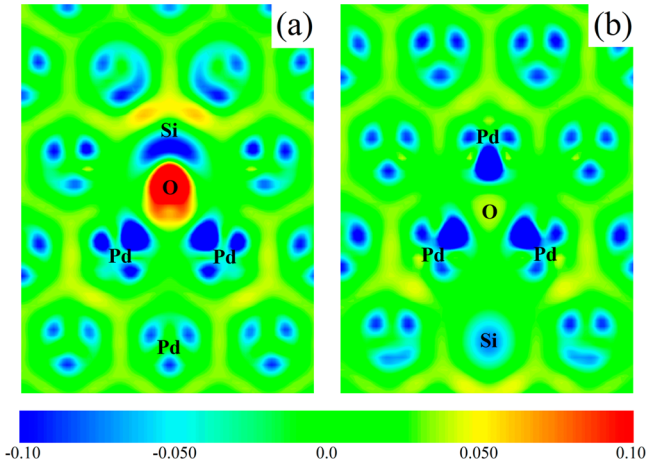

Figure 3. Bonding charge density distribution $\rho(\mathbf{r})$ on the Pd(111) surface. (a) a Si atom is at the 1st NN to the O atom. (b) Si atom is at the 2nd NN to the O atom.

(Figure 3b) to a Si atom. The positive (negative) value of $\rho(\mathbf{r})$ indicates charge accumulation (depletion) when the atoms are brought together to form the solid. When Si is the first NN to O, a strong ionic bonding is formed between them; hence, E_O is much lower than that on the pure Pd surface. When Si is the second NN to O, however, there is no apparent Si−O bonding. Rather, O bonds to nearby Pd atoms. To a less extent, Si also bonds to some of these Pd atoms. In other words, there is a competition between Si and O to bond with the Pd atoms. As a result, the Pd−O bonds are weakened (i.e., E_O is higher) as compared to the pure Pd surface. This explains the change of E_O in Figure 2d as well as the beneficial effect on ORR due to the second NN Si.

To examine the strain effect on ORR, we apply ±2% biaxial strain to the Pd(111) surface with either Cu or Si substitution. Consistent to the pioneering work of Mavrikakis et al.[23] we find that the compressions weaken the oxygen adsorption on the surface while the expansions strengthen it. Therefore, a compressive strain could enhance the ORR activity, and the combination of the substitution with straining offers a promising route to achieving superior ORR activities.

Pd−Cu−Si Metallic Glasses. In the following, we turn to the calculations of E_O on the Pd−Cu−Si metallic glasses to assess their potentials as ORR catalysts. This is a challenging task. On the one hand, the lack of crystalline symmetry in the glasses requires many more nonequivalent oxygen adsorption sites be considered. A distribution of E_O, $P(E_O)$, therefore has to be determined as opposed to a single E_O value on the crystalline surface. On the other hand, surface structures are not well-defined in the metallic glasses. Hence, in this work we first identify a local chemical environment of interest in the glass, and then cut the Pd-MG to create a surface with such local environment. For each Pd-MG, ∼70 surfaces are generated in this way and then relaxed to their local equilibrium structures. On each of the surfaces, one or two (deformed) fcc adsorption sites are randomly selected for E_O calculations. Thus, for each Pd-MG, ∼100 E_O energies are calculated to obtain the distribution function $P(E_O)$. In each of the calculations, there are 227−256 atoms in the DFT supercell. Figure S2 (Supporting Information) presents two atomic structures of Pd-MG surfaces as examples.

Figure 4 presents $P(E_O)$ for both Si_6 and Si_{17} Pd-MGs. To analyze the results, we classify the local environments around

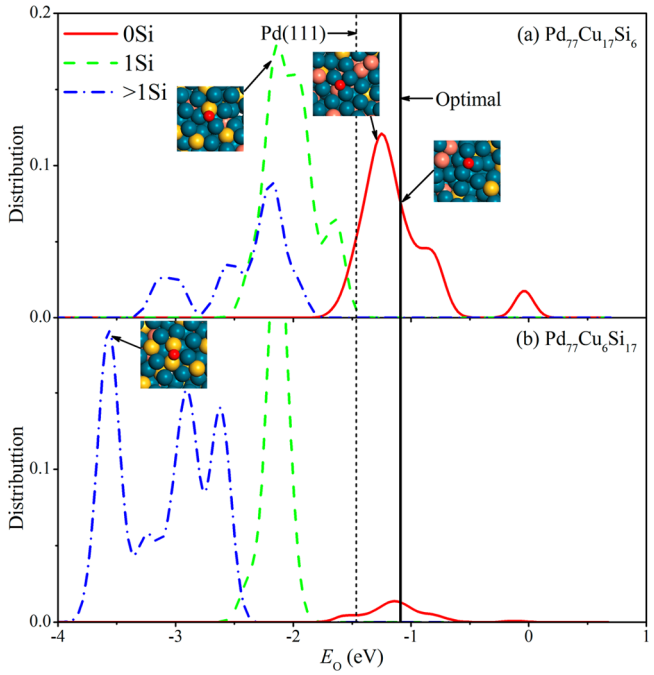

Figure 4. E_O distribution $P(E_O)$ for (a) Si_6 Pd-MG and (b) Si_{17} Pd-MG. The solid (red), dashed (green), and dot-dashed (blue) curves represent $P(E_O)$ at Si deficient sites (0Si), single-Si sites (1Si) and multi-Si sites (>1Si), respectively. The solid and dotted vertical lines represent the optimal E_O value and the E_O value on the Pd(111) surface, respectively. Some typical atomic structures around the adsorption site are shown.

an adsorption site in terms of the number of Si atoms present. If there is no NN Si atom surrounding the oxygen, the adsorption site is classified as Si-deficient (0Si); if there is only one NN Si atom to the oxygen, the adsorption site is classified as single-Si (1Si); if there are more than one NN Si atoms to the oxygen, the site is classified as multi-Si (>1Si). The $P(E_O)$ distributions are displayed in solid (red), dashed (green), and dotted-dash (blue) curves in Figure 4. $P(E_O)$ represents the probability of finding a given local environment on the glass surfaces with $E_O - dE_O < E_O < E_O + dE_O$. The area under each curve corresponds to the total probability of finding such local environment on the glass surfaces. Some of the typical local environments are also shown in the figure. One immediately notices that Si is detrimental to ORR since the curves move away from the optimal E_O (solid vertical line) as the local Si content is increased, consistent with the result on the crystalline surface and the experiment. In general the most stable adsorption sites are still the fcc-hollow positions, same as

dx.doi.org/10.1021/jp508636y | J. Phys. Chem. C 2014, 118, 28609−28615

those on the crystalline Pd(111) surface. More importantly, for Si_6 Pd-MG, the Si-deficient sites, which account to 31% of all adsorption sites considered, exhibit higher ORR activities than pure Pd, suggesting that low-Si metallic glasses are promising ORR catalysts. The reasons that the Si-deficient sites are more active than pure Pd are 2-fold: (1) as shown in Figure 2b, the substitution of Cu on the Pd surface could increase E_O. Hence the Pd-MG with 17% Cu exhibits a higher ORR activity than the pure Pd. (2) in the Pd-MG, the average NN Pd distance is 2.44 Å (Figure 1), which is smaller than that on the crystalline (111) surface (2.82 Å). In other words, there is a built-in compression in the Pd-MG which increases E_O, endowing it with a higher ORR activity than the crystalline Pd. For Si_{17} Pd-MG, we find that the number of the Si-deficient sites diminishes drastically (a 10-fold reduction) and the number of the Si-rich sites increases significantly. Owing to the low E_O values on these Si-rich sites, Si_{17} Pd-MG would not be a good ORR catalyst. Therefore, in developing Pd-based metallic glasses for ORR catalysts, one should minimize Si content if possible.

Effect of Strain. As alluded to in the introduction, metallic glasses can sustain very high elastic strains and stresses, thus opening an avenue to tune their catalytic activity via active straining. To confirm this, we compute the stress−strain relationship for Si_6 metallic glass under a uniaxial tension. The simulation is performed on a supercell of 53 × 53 × 214 $Å^3$ in x, y and z direction, respectively. Three-dimensional periodic boundary conditions are used with an *NPT* ensemble[48,49] at T = 30 K. The dimensions of the supercell in x and y direction are free to change but the dimension in z direction is fixed. For each strain increment in z direction, the system is thermalized in 50 ps, and then stress is calculated at every 5 ps. A total of 13 such stress values are averaged to arrive at a σ_{zz} for each strain increment; the stress−strain relationship is displayed in Figure 1c. We estimate that the tensile yield strain is 3.8% corresponding to a theoretical yield stress of 2.28 GPa. Therefore, we confirm that the Pd-MGs can indeed sustain very high elastic strains (∼10 times higher) compared with the crystalline counterparts. More importantly, since there is no dislocation in the glasses, the plastic deformation mechanism by which the metallic glasses relax the elastic strain is very different from that in a crystalline. It is thus expected that the elastic strain in metallic glasses cannot be as effectively relaxed as in the crystalline. As a result, the elastic strain on the metallic glass surface could be even higher than the yield strain as estimated here. However, more work needs to be done to understand the relaxation mechanism of elastic strain on the metallic glass surfaces and to provide more accurate estimate of the maximum elastic strain which can be harnessed for catalysis. Following the finding on the crystalline surface, we also apply compressions on the metallic glasses to drive E_O upward. To this end, we carry out *NVT* MD simulations with T = 300 K to estimate the maximum hydrostatic compression that the Pd-MGs can sustain. We monitor the change of the RDF $g(r)$ of the Pd-MGs under the strain, and estimate the maximal compression as 6%. As presented in Figure 1c, for both Pd-MGs, $g(r)$ displays similar characteristics under the compressions with the peaks shifting toward shorter distances. There is no sudden or drastic change to $g(r)$, suggesting that the metallic glasses maintain their structural integrity under the strains. In addition, we have carefully examined the MD snapshots, but have not noticed the formation of any extended defects.

In order to examine the general behavior of strain-dependence of E_O, we apply a biaxial compression of 3%, 4.5%, and 6% to the Pd-MGs and the results are shown in Figure 5. Although these compressions are greater in value than

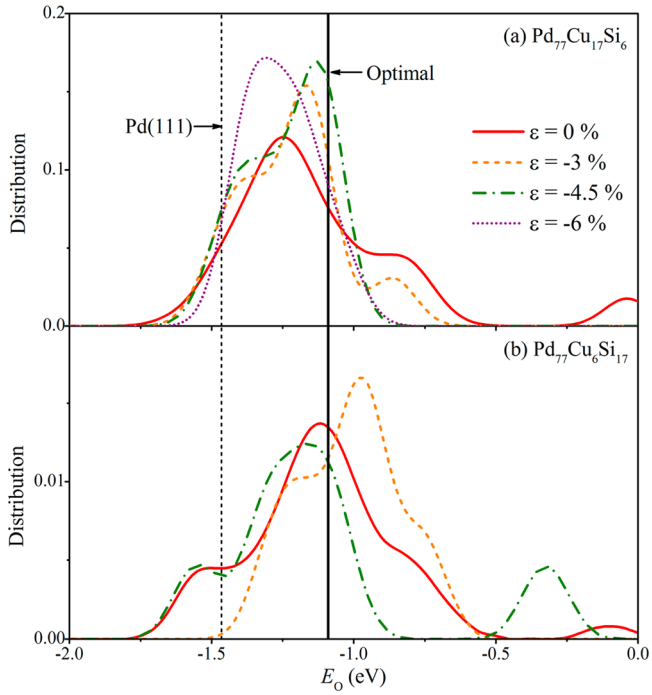

Figure 5. $P^{0Si}(E_O)$ of (a) Si_6 Pd-MG and (b) Si_{17} Pd-MG under different biaxial compressions. Note the different vertical scales between part a and b.

the tensile yield strain estimated from the simulations, they could be potentially harnessed owing to the lack of dislocations in the metallic glasses. Here we only focus on the Si-deficient sites because they are the active sites for ORR; the Si-rich sites are considered "poisoned" and cannot contribute substantially to the ORR activity even under strains. For both glasses, we find the strain dependence to be bimodal. For Si_6 Pd-MG, if the compression is not overly large (∼4.5%), it raises E_O consistent with the known trend. However, if the compression is too large (6%), it reverses the trend and lowers E_O. The fact that the $P(E_O)$ peaks become higher (i.e., with more active sites) and shift toward to the optimal E_O suggests that the ORR activity on the Si_6 MG would increase substantially under a compression of 3 to 4.5%. Hence a low Si-content Pd-MG under compression could surpass the ORR activity of pure Pd and approach the ORR activity of Pt. For Si_{17} Pd-MG, the compressions do not appear to improve its ORR activity: a compression of 3.0% overshoots the optimal value and a compression of 4.5% moves the energy to the opposite direction, away from the optimal value. Therefore, the high Si-content Pd-MG remains as an inferior ORR catalyst despite the stress. To understand the bimodal strain dependence, we return to the crystalline Pd surface and calculate E_O as a function of compression. The results are shown in Figure 6. Since the surface model contains only four atomic layers, it is too thin to nucleate dislocations. As a result, a large strain up to 8% compression can be accommodated in this unrealistic model. But here we are only concerned of chemistry, i.e., E_O dependence on strain, not of the mechanical responses of the surface. We note that E_O rises monotonically as the strain is

dx.doi.org/10.1021/jp508636y | J. Phys. Chem. C 2014, 118, 28609−28615

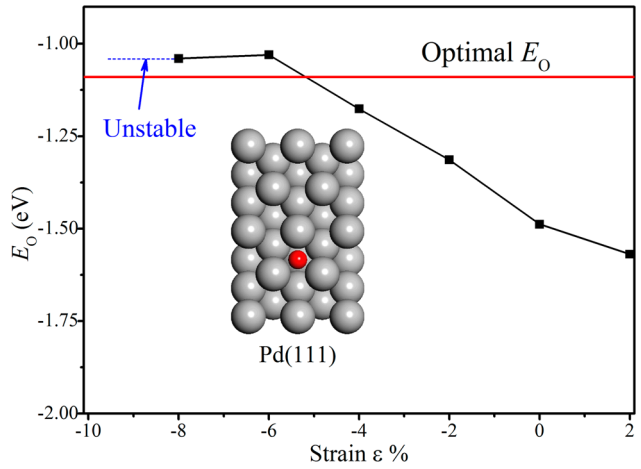

Figure 6. E_O as a function of biaxial surface strain for the pure Pd(111) surface. The small red sphere represents the O atom.

increased. However, as the compression exceeds 6%, E_O starts declining (beyond 8% compression, no relaxed atomic structure can be obtained). This explains the bimodal behavior observed in the metallic glasses and provides an estimate for the optimal compression on the metallic glasses. Since the NN Pd−Pd distance in the crystalline surface is larger than that in the Pd-MGs (2.82 vs 2.44 Å), the optimal compression (5%) for the metallic glass surfaces would be proportionally smaller than that for the crystalline surface (6%).

CONCLUSION

In summary, we have performed first-principles calculations to assess the ORR activity of Pd-MGs based on the oxygen adsorption energy E_O. It is found that the substitution of Cu for Pd on the crystalline Pd(111) surface enhances the ORR activity. Although there exist local adsorption structures where the substitution of Si for Pd could render more active ORR, in general Si is poisonous to ORR because it bonds too strongly to oxygen, consistent with the experimental observations. Compressive strains are found to weaken oxygen binding on the surface and to enhance the ORR activity. With two Pd-based metallic glasses as examples, we explore the potential of Pd−Cu−Si metallic glasses as ORR catalysts based on the analysis of E_O distribution. We find that for the Si-deficient adsorption sites, the local ORR activity could exceed that of pure Pd, while the Si-rich sites render a rather poor ORR activity. Si in Pd-MGs is detrimental to the ORR activity and thus should be minimized. The Pd-MGs can sustain a much higher compression than the crystalline counterpart and under an optimal compression (5%), the ORR activity on the Si-deficient adsorption sites could exceed that of pure Pd. We predict that Pd-MGs with low Si contents are potential candidates for Pt-free ORR catalysts.

ASSOCIATED CONTENT

Supporting Information

Cyclic voltammetry experimental details and cyclic voltammetry curves for the ORR for Pd−Si binary alloys, atomic coordinations of Pd(111), and metallic glass surface and segregation energy of Si in metllic glasses. This material is available free of charge via the Internet at http://pubs.acs.org.

AUTHOR INFORMATION

Corresponding Author

*(G.L.) E-mail: ganglu@csun.edu. Telephone: (+1) 818-677-2012.

Notes

The authors declare no competing financial interest.

ACKNOWLEDGMENTS

We thank Howard Sheng, William Curtin, Pradeep Guduru, and Xu Zhang for valuable discussions. This work was supported by the Army Research Office through Grant W911NF-11-1-0353.

REFERENCES

(1) Mukerjee, S.; Srinivasan, S. Enhanced Electrocatalysis of Oxygen Reduction on Platinum Alloys in Proton Exchange Membrane Fuel Cells. *J. Electroanal. Chem.* **1993**, *357*, 201−224.
(2) Wang, C.; Waje, M.; Wang, X.; Tang, J. M.; Haddon, R. C.; Yan, Y. Proton Exchange Membrane Fuel Cells with Carbon Nanotube Based Electrodes. *Nano Lett.* **2004**, *4*, 345−348.
(3) Wang, Y.; Zhou, H. A Lithium-air Battery with a Potential to Continuously Reduce O_2 from Air for Delivering Energy. *J. Power Sources* **2010**, *195*, 358−361.
(4) Christensena, J.; Albertusa, P.; Sanchez-Carrerab, R. S.; Lohmanna, T.; Kozinskyb, B.; Liedtkec, R.; Ahmeda, J.; Kojica, A. A Critical Review of Li/Air Batteries. *J. Electrochem. Soc.* **2012**, *159*, R1−R30.
(5) Ferreira, P. J.; la O', G. J.; Shao-Horn, Y.; Morgan, D.; Makharia, R.; Kocha, S.; Gasteiger, H. A. Instability of Pt/C Electrocatalysts in Proton Exchange Membrane Fuel Cells: A Mechanistic Investigation. *J. Electrochem. Soc.* **2005**, *152*, A2256−A2271.
(6) Zhang, J.; Sakaki, K.; Sutter, E.; Adzic, R. R. Stabilization of Platinum Oxygen-Reduction Electrocatalysts Using Gold Clusters. *Science* **2007**, *315*, 220−222.
(7) Chen, Z. W.; Waje, M.; Li, W. Z.; Yan, Y. S. Supportless Pt and PtPd Nanotubes as Electrocatalysts for Oxygen-Reduction Reactions. *Angew. Chem., Int. Ed.* **2007**, *46*, 4060−4063.
(8) Gu, X.; Xu, L.; Tian, F.; Ding, Y. Au-Ag Alloy Nanoporous Nanotubes. *Nano. Res.* **2009**, *2*, 386−393.
(9) Liu, L.; Pippel, E.; Scholz, R.; Gosele, U. Nanoporous Pt-Co Alloy Nanowires: Fabrication, Characterization, and Electrocatalytic Properties. *Nano Lett.* **2009**, *9*, 4352−4358.
(10) Zhang, C.; Xu, L.; Shan, N.; Sun, T.; Chen, J.; Yan, Y. Enhanced Electrocatalytic Activity and Durability of Pt Particles Supported on Ordered Mesoporous Carbon Spheres. *ACS Catal.* **2014**, *4*, 1926−1930.
(11) Carmo, M.; Sekol, R. C.; Ding, S.; Kumar, G.; Schroers, J.; Taylor, A. D. Bulk Metallic Glass Nanowire Architecture for Electrochemical Applications. *ACS Nano* **2011**, *5*, 2979−2983.
(12) Liu, Y. H.; Wang, G.; Wang, R. J.; Zhao, D. Q.; Pan, M. X.; Wang, W. H. Super Plastic Bulk Metallic Glasses at Room Temperature. *Science* **2007**, *315*, 1385−1388.
(13) Gludovatz, B.; Demetriou, M. D.; Floyd, M.; Hohenwarter, A.; Johnson, W. L.; Ritchie, R. O. Enhanced Fatigue Endurance of Metallic Glassis through a Stair-case-like Fracture Mechanism. *Proc. Natl. Acad. Sci. U.S.A.* **2013**, *110*, 18419−18424.
(14) Schroers, J. Processing of Bulk Metallic Glass. *Adv. Mater.* **2010**, *22*, 1566−1569.
(15) Hirata, A.; Kang, L. J.; Fujita, T.; Klumov, B.; Matsue, K.; Kotani, M.; Yavari, A. R.; Chen, M. W. Geometric Frustration of Icosahedron in Metallic Glasses. *Science* **2013**, *341*, 376−379.
(16) Kumar, V.; Fujita, T.; Konno, K.; Matsuura, M.; Chen, M.; Inoue, A.; Kawazoe, Y. Atomic and Electronic Structure of $Pd_{40}Ni_{40}P_{20}$ Bulk Metallic Glass from ab Initio Simulations. *Phys. Rev. B* **2011**, *84*, 134204.
(17) Chen, H. S. Thermodynamic Considerations on the Formation and Stability of Metallic Glasses. *Acta Metall.* **1974**, *22*, 1505−1511.

(18) Inoue, A. Stabilization of Metallic Supercooled Liquid and Bulk Amorphous Alloys. *Acta Mater.* **2000**, *48*, 279−306.
(19) Inoue, A.; Takeuchi, A. Recent Development and Application Products of Bulk Glassy Alloys. *Acta Mater.* **2011**, *59*, 2243−2267.
(20) Nishiyama, N.; Inoue, A. Stability and Nucleation Behavior of Glass-forming Pd-Cu-Ni-P Alloy with a Critical Cooling Rate of 0.067 K/s. *Intermetallics* **2002**, *10*, 1141−1147.
(21) Wang, X.; Kariuki, N.; Vaughey, J.; Goodpaster, J.; Kumar, R.; Myers, D. Bimetallic Pd-Cu Oxygen Reduction Electrocatalysts. *J. Electrochem. Soc.* **2008**, *155*, B602−B609.
(22) Founda-Onana, F.; Bah, S.; Savadogo, O. Palladium-copper Alloys as Catalysts for the Oxygen Reduction Reaction in an Acidic Media 1: Correlation between the ORR Kinetic Parameters and Intrinsic Physical Properties of the Alloys. *J. Electroanal. Chem.* **2009**, *636*, 1−9.
(23) Mavrikakis, M.; Hammer, B.; Nørskov, J. K. Effect of Strain on the Reactivity of Metal Surfaces. *Phys. Rev. Lett.* **1998**, *81*, 2819−2822.
(24) Chen, M. W. Mechanical Behavior of Metallic Glasses: Microscopic Understanding of Strength and Ductility. *Annu. Rev. Mater. Res.* **2008**, *38*, 445−469.
(25) Schroers, J.; Johnson, W. Ductile Bulk Metallic Glass. *Phys. Rev. Lett.* **2004**, *93*, 255506.
(26) Shi, Y.; Falk, M. L. Stress-induced Structural Transformation and Shear Banding during Simulated Nanoindentation of a Metallic Glass. *Acta Mater.* **2007**, *55*, 4317−4324.
(27) Chen, Z. P.; Gao, J. E.; Wu, Y.; Wang, H.; Liu, X. J.; Lu, Z. P. Designing Novel Bulk Metallic Glass Composites with a High Aluminum Content. *Sci. Rep.* **2013**, *3*, 3353.
(28) Nørskov, J. K.; Rossmeisl, J.; Logadottir, A.; Lindqvist, L.; Kitchin, J. R.; Bligaard, T.; Jónsson, H. Origin of the Overpotential for Oxygen Reduction at a Fuel-Cell Cathode. *J. Phys. Chem. B* **2004**, *108*, 17886−17892.
(29) Zhang, J. L.; Vukmirovic, M. B.; Xu, Y.; Mavrikakis, M.; Adzic, R. R. Controlling the Catalytic Activity of Platinum-Monolayer Electrocatalysts for Oxygen Reduction with Different Substrates. *Angew. Chem., Int. Ed.* **2005**, *44*, 2132−2135.
(30) Stamenkovic, V.; Mun, B. S.; Mayrhofer, K. J.; Ross, P. N.; Marković, N. M.; Rossmeisl, J.; Greeley, J.; Nørskov, J. K. Changing the Activity of Electrocatalysts for Oxygen Reduction by Tuning the Surface Electronic Structure. *Angew. Chem., Int. Ed.* **2006**, *45*, 2897−2901.
(31) Stamenkovic, V. R.; Fowler, B.; Mun, B. S.; Wang, G. F.; Ross, P. N.; Lucas, C. A.; Marković, N. M. Improved Oxygen Reduction Activity on $Pt_3Ni(111)$ via Increased Surface Site Availability. *Science* **2007**, *315*, 493−496.
(32) Greeley, J.; Stephens, I. E. L.; Bondarenko, A. S.; Johansson, T. P.; Hansen, H. A.; Jaramillo, T. F.; Rossmeisl, J.; Chorkendorff, I.; Nørskov, J. K. Alloys of Platinum and Early Transition Metals as Oxygen Reduction Electrocatalysts. *Nat. Chem.* **2009**, *1*, 552−556.
(33) Nørskov, J. K.; Bligaard, T.; Logadottir, A.; Bahn, S.; Hansen, L. B.; Bollinger, M.; Bengaard, H.; Hammer, B.; Sljivancanin, Z.; Mavrikakis, M.; et al. Universality in Heterogeneous Catalysis. *J. Catal.* **2002**, *209*, 275−278.
(34) Abild-Pedersen, F.; Greeley, J.; Studt, F.; Rossmeisl, J.; Munter, T. R.; Moses, P. G.; Skúlason, E.; Bligaard, T.; Nørskov, J. K. Scaling Properties of Adsorption Energies for Hydrogen-Containing Molecules on Transition-Metal Surfaces. *Phys. Rev. Lett.* **2007**, *99*, 016105.
(35) Zhang, S.; Zhang, X.; Jiang, G. M.; Zhu, H.; Guo, S. J.; Su, D.; Lu, G.; Sun, S. H. Tuning Nanoparticle Structure and Surface Strain for Catalysis Optimization. *J. Am. Chem. Soc.* **2014**, *136*, 7734−7739.
(36) Plimpton, S. J. Fast Parallel Algorithms for Short-Range Molecular Dynamics. *J. Comput. Phys.* **1995**, *117*, 1−19. http://lammps.sandia.gov.
(37) Cheng, Y. Q.; Ma, E.; Sheng, H. Atomic Level Structure in Multicomponent Bulk Metallic Glass. *Phys. Rev. Lett.* **2009**, *102*, 245501.
(38) Sheng, H. W.; Kramer, M. J.; Cadien, A.; Fujita, T.; Chen, M. W. Highly Optimized Embedded-Atom-Method Potentials for Fourteen FCC Metals. *Phys. Rev. B* **2011**, *83*, 134118.
(39) Hoover, W. G. Canonical Dynamics: Equilibrium Phase-space Distributions. *Phys. Rev. A* **1985**, *31*, 1695−1697.
(40) Kajita, S.; Kohara, S.; Onodera, Y.; Fukunaga, T.; Matsubara, E. Structural Analysis of Pd-Cu-Si Metallic Glassy Alloy Thin Films with Varying Glass Transition Temperature. *Mater. Trans.* **2011**, *52*, 1349−1355.
(41) Perdew, J. P.; Burke, K.; Ernzerhof, M. Generalized Gradient Approximation Made Simple. *Phys. Rev. Lett.* **1996**, *77*, 3865−3868.
(42) Perdew, J. P.; Burke, K.; Ernzerhof, M. Perdew, Burke, and Ernzerhof Reply. *Phys. Rev. Lett.* **1998**, *80*, 891.
(43) Blöchl, P. E. Projector Augmented-Wave Method. *Phys. Rev. B* **1994**, *50*, 17953−17979.
(44) Kresse, G.; Hafner, J. Ab Initio Molecular Dynamics for Liquid Metals. *Phys. Rev. B* **1993**, *47*, 558−561(R).
(45) Kresse, G.; Furthmüller, J. Efficient Iterative Schemes for ab Initio Total-energy Calculations Using a Plane-wave Basis Set. *Phys. Rev. B* **1996**, *54*, 11169−11186.
(46) Monkhorst, H. J.; Pack, J. D. Special Points for Brillouin-zone Integrations. *Phys. Rev. B* **1976**, *13*, 5188−5192.
(47) Tang, W. J.; Zhang, L.; Henkelman, G. Catalytic Activity of Pd/Cu Random Alloy Nanoparticles for Oxygen Reduction. *J. Phys. Chem. Lett.* **2011**, *2*, 1328−1331.
(48) Martyna, G.; Tobias, D.; Klein, M. Constant Pressure Molecular Dynamics Algorithms. *J. Chem. Phys.* **1994**, *101*, 4177−4189.
(49) Tuckerman, M.; Alejandre, J.; López-Rendón, R.; Jochim, A.; Martyna, G. A Liouville-operator Derived Measure-preserving Integrator for Molecular Dynamics Simulations in the Isothermal-isobaric Ensemble. *J. Phys. A: Math. Gen.* **2006**, *39*, 5629−5651.